SOILS AND FOUNDATIONS Vol. 51, No. 6, 1091–1102, Dec. 2011
Japanese Geotechnical Society

CENTRIFUGE MODELING ON MANHOLE UPLIFT IN A LIQUEFIED TRENCH

TETSUO TOBITA[i], GI-CHUN KANG[ii] and SUSUMU IAI[iii]

ABSTRACT

The uplift behavior of sewage manholes due to liquefaction in a trench is investigated through a series of dynamic centrifuge model tests. The objectives of a series of tests are to study the mechanism of the uplift and to obtain relationships among uplift displacement and factors affecting the uplift. The factors considered in the experiments are the ground water levels, the magnitude of input accelerations, the duration time of shaking, the relative densities of trench backfill and the native ground, the material of native ground, the volume of a trench, the apparent unit weight of a manhole, and the contact conditions at the bottom of a manhole. Test results show that the primary cause of uplift is the reduction of the effective confining stress near the bottom of a manhole due to strong shaking. The magnitude of uplift is found to be strongly correlated with the ground water depth, the intensity of shaking, the shear deformation of the trench, and the contact conditions at the bottom of the manhole. These findings are believed to be useful for engineering practice in the mitigation of the manhole uplift.

Key words: centrifuge modeling, earthquakes, liquefaction, manhole, uplift (**IGC**: E7/F7/H8)

INTRODUCTION

With the continued sprawling of cities and growing populations, residential areas are spreading into suburban areas, with a consequent increase in the number of sewage manholes damaged after large earthquakes. The uplifting phenomenon of sewerage manholes was reported after the 1964 Niigata, Japan, earthquake (Okamoto, 1984; JGS, 2003; Wakamatsu, 2007), the 1993 Kushiro-oki (JSSMFE, 1994; Koseki et al., 1997), the 2003 Tokachi-oki (JGS, 2004; Yasuda et al., 2004), the 2004 Niigataken Chuetsu (Yasuda and Kiku, 2006), the 2007 Niigataken Chuetsu-oki (Tobita et al., 2007), and the 2010 Maule, Chile, earthquake (Yasuda et al., 2010). For example, more than 1,400 manholes were damaged after the 2004 Niigataken Chuetsu, Japan, earthquake (Yasuda and Kiku, 2006) (Fig. 1). Damaged manholes not only cause serious problems for citizens' daily lives but also hinder road traffic after earthquakes.

Fig. 1. Uplifted manhole after the 2004 Niigata-ken Chuetsu, Japan, earthquake

In the course of the construction of sewerage manholes, the ground is excavated, and the trench is backfilled with sandy material because of its ease of handling after placing the manholes. It has been known that the liquefaction of backfill soils may cause the uplift of manholes (Koseki et al., 1997; Yasuda and Kiku, 2006). Field investigations (Kiku, 2004; Yasuda, 2005; Yasuda and Kiku, 2006; Yasuda et al., 2009), small-scale model tests (Ohtomo et al., 1987; Yasuda et al., 1995; Koseki et al., 1997; Koseki et al., 1998), and numerical analyses (Iai and Matsunaga, 1991; JGS, 2003) have been conducted to reveal the cause and mechanism of the uplift. Based on those results, the mechanism of uplift is explained as follows. First, the uplifting force is initiated by the increase in excess pore water pressure due to the liquefaction of

[i] Assistant Professor, Disaster Prevention Research Institute, Kyoto University, Japan (tobita.tetsuo.8e@kyoto-u.ac.jp).
[ii] Researcher, ditto.
[iii] Professor, ditto.
The manuscript for this paper was received for review on December 6, 2010; approved on July 10, 2011.
Written discussions on this paper should be submitted before July 1, 2012 to the Japanese Geotechnical Society, 4-38-2, Sengoku, Bunkyo-ku, Tokyo 112-0011, Japan. Upon request the closing date may be extended one month.

the backfill caused by strong shaking. Then, liquefied backfill flows beneath a manhole because the apparent unit weight of a manhole is normally smaller than that of the backfill, which causes a gradient of initial effective overburden pressure at the depth of the manhole base. Uplifting continues until equilibrium is achieved between the uplifting force, the weight of the manhole, friction, and resistance from sewage pipes connected to the manhole. Based on this equilibrium, the safety factor against uplift is derived. Koseki et al. (1997) examined the relationship between the safety factor and the uplift displacement of box-type structures and manholes. They concluded that the uplift of underground structures continues when the safety factor is almost equal to or less than 1.0, and that the safety factor can be used to evaluate whether uplift is triggered or not. This factor, however, only yields the triggering condition of uplift and is incapable of predicting the amount of uplift. Tobita et al. (2010) proposed a method to predict the maximum uplift displacement of a manhole and trench-backfill settlement due to liquefaction considering static equilibrium of forces. To the conventional equilibrium forces, their method adds a number of variables: uplift displacement, Δf, and the settlement of backfill, Δs, under the condition where the volume of an uplifted portion of a manhole is equal to the settled volume of a trench backfill. With the experimental results reported in this study, their method successfully predicts the maximum uplift displacement of a manhole.

In the present study, 21 centrifuge model tests in total are conducted to identify factors affecting the liquefaction-induced manhole uplift. Factors considered in the tests are as follows: (a) the depth of the ground water table, (b) the amplitude of input acceleration, (c) the number of load cycles, (d) the relative density of backfill, (e) a cross-sectional area of a trench, (f) the apparent unit weight of the manhole, (g) the condition of the native ground, and (h) the contact conditions between the bottom of a manhole and the trench.

Note that, in order to evaluate the effectiveness of mitigation measures against uplift, model manholes with some sort of mitigation devices are tested simultaneously with a model manhole of no mitigation devices attached. However, this paper will focus on the test cases with manholes containing no mitigation measures. Test results with mitigation measures have been discussed in Kang (2010) and will be published elsewhere.

CENTRIFUGE MODEL AND TEST DESCRIPTION

The geotechnical centrifuge at the Disaster Prevention Research Institute, Kyoto University, Japan, was employed for the series of tests conducted in this study. The centrifuge facility has an in-flight platform radius of 2.5 m and a capacity of 24 g-ton. It is equipped with a one-dimensional shake table (allowable displacement: ± 5 mm), which is operable under the centrifugal accelerations of up to 50 g. It has a single servo hydraulic actuator parallel to the rotation of the centrifuge arm, and it is controlled through a laptop personal computer (PC) on the centrifuge arm. The PC is fixed near the rotation axis of the centrifuge to minimize the centrifugal force acting on it. It is connected to a PC in the control room by a wireless LAN, and the data loggers attached on the arm are accessible from a PC in the control room through a wireless USB connection. A counter-weight is loaded on the other side of the arm to maintain balance during rotation. Using the CCD camera mounted on the swinging arm, the lateral side of the model can be monitored through a glass wall of the sandbox.

Details of the Model Manhole

The target manhole is the standard No. 1 manhole (Fig. 2), which is a precast manhole typically used in Japan (JSWA, 2001). It consists of four parts: a ring and cover on top, a manhole cone, a shaft, and a base slab with inlet and outlet. Properties of the target No. 1 manhole are shown in Fig. 2. Two model manholes are used in the tests, both made of aluminum cylinders whose dimensions are shown in Figs. 3(a) and (b), and Table 1. For simplicity, the manhole cone, inlet and outlet are not taken into consideration. Both models have an outer diameter of 55 mm and a wall thickness of 5 mm in model scale. The long manhole length is 150 mm (Fig. 3(a)), while the short one is 100 mm in length (Fig. 3(b)) in the model scale. They are referred to a Models No. 1 and No.

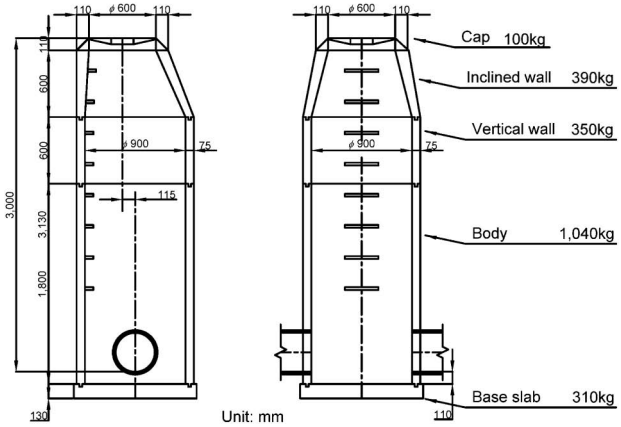

Fig. 2. Cross section of the standard No. 1 manhole (JSWA, 2001)

Table 1. Properties of model manhole (in prototype scale)

Aluminum	Unit weight		γ_a	26.5 kN/m^3
Model manhole	Diameter		d	1.1 m
	Wall thickness		t	0.1 m
	Mass of sensors installed with manhole		W_s	0.67 kN
	Mass of base slab		W_{base}	1.7 kN
	Length, $h=3$ m	Total weight	W_t	27.3 kN
		Volume	V	2.85 m^3
		Apparent unit weight	γ_m	9.57 kN/m^3
	Length, $h=2$ m	Total weight	W_t	18.98 kN
		Volume	V	1.90 m^3
		Apparent unit weight	γ_m	9.98 kN/m^3

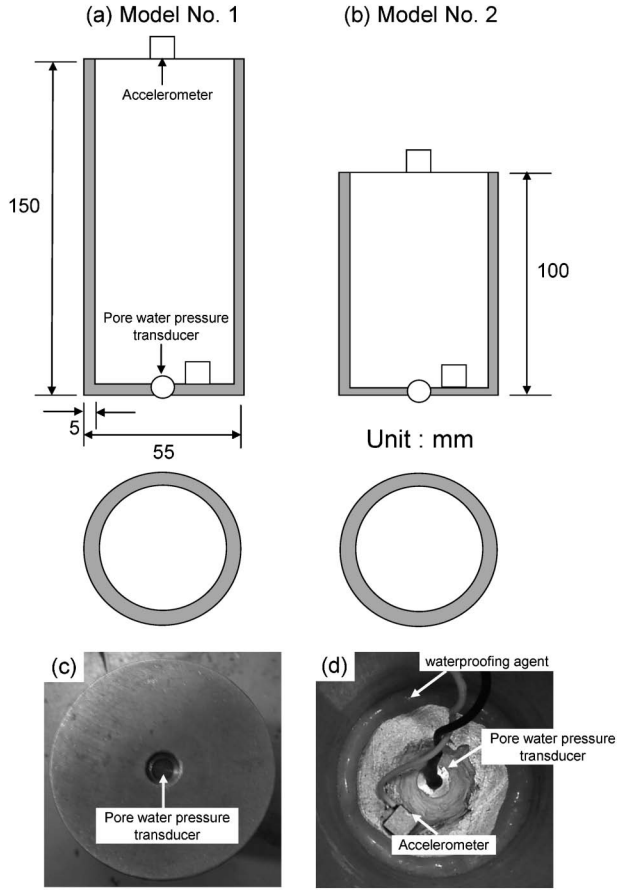

Fig. 3. Dimension of model manholes (in model scale): (a) Model No. 1 with 150-mm length, (b) Model No. 2 with 100-mm length, (c) outside view of the bottom of the model manhole, and (d) inside view of the model manhole

Table 2. Properties of silica sand

Specific gravity	G_s	2.66
D_{50}		0.172 mm
D_{10}		0.110 mm
Cofficient of uniformity	C_u	1.727
Cofficient of curvature	C_g	0.938
Maximum void ratio	e_{max}	1.19
Minimum void ratio	e_{min}	0.71
Wet sand	γ_t	14.8 kN/m^3
Saturated sand	γ_{sat}	18.1 kN/m^3

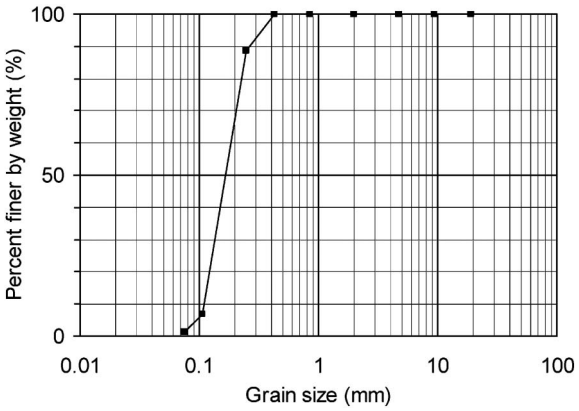

Fig. 4. Grain size distribution curve for silica sand

2, as indicated in Figs. 3(a) and (b). The apparent unit weight of Model No. 1 is 9.57 kN/m^3, including the sensors mounted inside, and that of Model No. 2 is 9.98 kN/m^3. Figures 3(c) and (d) show the pore water pressure transducer and accelerometer installed at the bottom of the model manhole.

Preparation of the Viscous Fluids

Pore fluid having viscosity greater than that of water is used to satisfy the scaling law of the diffusion process of water in soil. With the Metolose (Shin-Etsu Chemical Co., 1997), a specified viscosity level can be achieved without changing any other significant fluid parameters, such as density or surface tension. Its effectiveness has been tested and confirmed up to 100 mPa s (Dewoolkar, et al., 1999). The Metolose used in this study is the Type SM-100 in the form of a white powder. It is tasteless, odorless, and physiologically harmless, but its viscosity is quite sensitive to temperature change. The major effect of viscous water on manhole uplift may be the friction exerted on the lateral side of the manhole. After three sets of strain-controlled triaxial tests, Dewoolkar et al. (1999) showed that overall constitutive behavior of the sand they used was not significantly altered by the use of Metolose instead of water as the pore fluid. Thus, the effect of the viscosity of Metolose on the model manhole uplift was assumed to be negligible. However, lubricant effects between sand and aluminum surface may need to be investigated in the future. In this study, a 2% solution of the Metolose, which has a viscosity of 100 mPa s at 20°C, was produced before model preparation. Then, the solution of 100 mPa s was diluted with water to obtain a viscosity of 20 mPa s at room temperature. A ''cup and bob''-type viscometer (Viscotester, VT03-F (RION Co., 1997)) is employed to measure the viscosity. Before model construction, the solution is de-aired in a vacuum chamber for approximately 24 hours until no air bubbles appeared at the water surface. Monitoring and adjusting the temperature in the solution is important for maintaining the specified viscosity of the pore water. For this purpose, a probe-like digital thermometer is embedded in the model ground, and the temperature of the model ground is adjusted by operating an air conditioner in the centrifuge chamber.

Model Construction

Silica sands are used to make the model ground. The physical properties of the sand are listed in Table 2, and the grain-size distribution curve is shown in Fig. 4. The soil is classified into ''poorly graded sand (SP).'' Crashed stones whose particle diameter varies approximately from 5 to 10 mm are placed under the model manhole. In a test case, low plasticity silt called ''DL Clay'' which is available in industry is mixed with sand to change properties of the native ground. The model ground is prepared in a

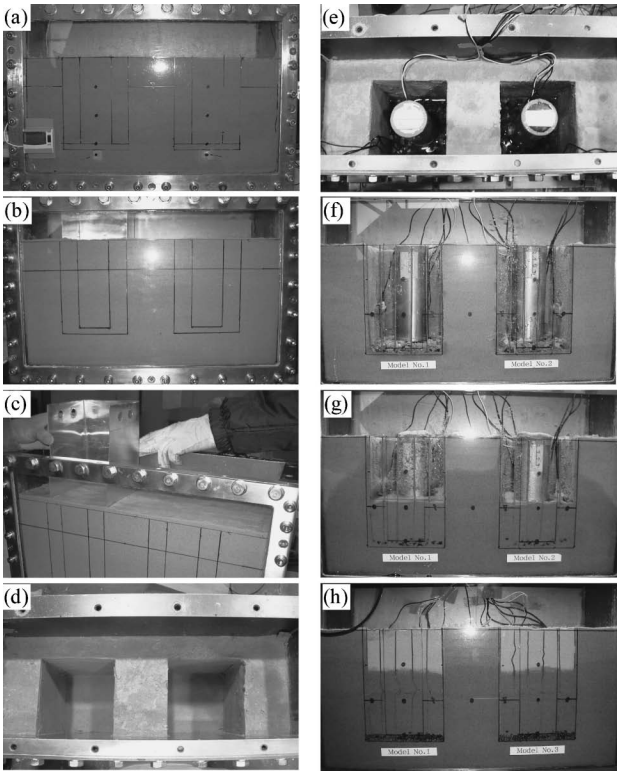

Fig. 5. Construction procedure of the model ground

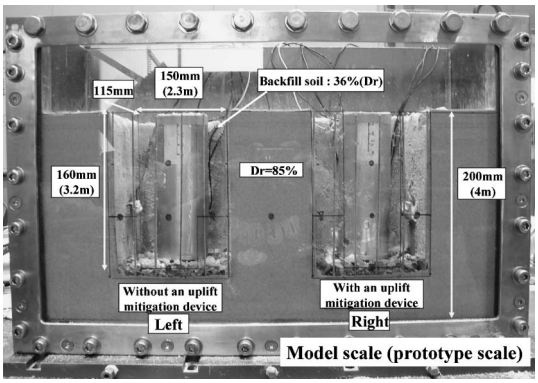

Fig. 6. Representative cross section of the model ground and manholes for CS1 to CS12

strongbox, with nominal inside dimensions of $0.45 \times 0.15 \times 0.30$ m with a glass wall on one side of the box. Note, in Figs. 5 and 6, that the two manholes are installed side by side. In these figures, no mitigation device is attached to the left manhole model, while, to the right one, some mitigation measures against uplift are installed.

The model ground is constructed as follows.

1. The layer of native ground with relative density, $Dr \approx 85\%$, is first prepared by compacting moist silica sands up to 200 mm (model scale) from the bottom of the container (Fig. 5(a)).
2. Then, to install the model manholes, a trench with a volume of $0.115 \times 0.115 \times 0.160$ m (model scale) is excavated using an aluminum mold of the same dimensions with a perimeter of the trench to prevent the reclaimed surface from collapsing during excavation (Figs. 5(b)–(d)).
3. The manhole is placed on top of a gravel layer of 10-mm thickness (Figs. 5(e)–(f)).
4. After saturating the native ground up to the specified ground water table with viscous water, the same silica sand with the native ground is water-pluviated in the trench as a backfill whose relative density is approximately 36% (Figs. 5(g)–(h), and Table 3).

From constant-head permeability tests, the permeability of silica sand with the distilled water is 3.64×10^{-3} cm/s for $Dr = 85\%$ and 8.80×10^{-3} cm/s for $Dr = 36\%$. Because of this permeability difference (2.4 times) between native ground and backfill, seepage of water from the backfill to the native ground is expected to be minor during shaking.

In each test, the model is prepared carefully so that the initial conditions of every experiment are nearly identical. Special care is taken for the saturation of the model ground. Namely, after constructing the model, viscous water is added to assure the full saturation of the native ground as well as backfill so that the water poured in the trench is not absorbed in the native ground.

Instrumentation and Measurement

To monitor the dynamic behavior of the model, 8 accelerometers, 8 pore water pressure transducers, and 2 laser displacement transducers are installed at each location specified in Fig. 7. Uplift displacement of the manholes is measured with D1, which has a capacity of ± 25 mm at a distance of 80 mm from the target. In addition to the measurements by the laser displacement sensors, uplift displacement is also measured by hand with a ruler to determine the final uplift displacement (Fig. 8). Because measurement by hand with a ruler was done in a 1-g field after stopping the centrifuge, the model manhole might have settled due to excess pore water pressure dissipation. Therefore, the values are systematically smaller than those of laser displacement transducers (Table 4). The ground surface settlements were also directly measured with a ruler before and after each experiment. The pore water pressure transducer P1 is placed in the backfill at a depth of GL. -2 m, and P2 is in the backfill at the same depth as the bottom of the manhole (GL. -3 m). P3 is attached at the bottom of the manhole from the inside to monitor the pore water pressure during uplift. P7 is located in the native ground at a depth of 4.0 m below the manholes.

Test Procedures

After confirming that all equipment and sensors are functioning well without any abnormalities, centrifugal acceleration is increased gradually up to 20 g. To properly consolidate the model ground before shaking, the model is put under 20 g for 5 minutes. The actual relative densities of the ground and the backfill after the consolidation are listed in Table 3. Due to the consolidation mentioned above, the relative density of backfill was increased from 36% to approximately 39%, while the ones

Table 3. Summary of the centrifuge tests

Test No.	Type of model manhole	Length of the manhole	(a) GWL	(b) Max. Amp. of inpu acceleration	(c) Number of load cycles	(d) Relative density Backfill soil	(g) Relative density Native ground	(e) Cross-sectional area of trench	(f) Appparent unit weight of manhole	(h) Contact condition at the bottom of manhole
	No.	m	m	m/s^2		%	%	m^3	kN/m^3	
1	1	3	0	6.78	30	38.7	85	2.3×2.3×3.0	9.57	Gravel
2	1	3	1	7.25	30	37.9	85	2.3×2.3×3.0	9.57	Gravel
3	1	3	1	7.15	30	38.7	85	2.3×2.3×3.0	9.57	Gravel
4	1	3	1.7	7.19	30	38.4	85	2.3×2.3×3.0	9.57	Gravel
5	1	3	3	6.60	30	37.3	85	2.3×2.3×3.0	9.57	Gravel
6	1	3	1	2.05	30	37.2	85	2.3×2.3×3.0	9.57	Gravel
7	1	3	1	4.64	30	38.7	85	2.3×2.3×3.0	9.57	Gravel
8	1	3	1	6.97	30	37.1	37.1	4.5×3.0×3.0	9.57	Gravel
9	1	3	1	6.47	30	85	85	2.3×2.3×3.0	9.57	Gravel
10	1	3	1	6.87	15	39.4	85	2.3×2.3×3.0	9.57	Gravel
11	1	3	1	6.91	60	38.1	85	2.3×2.3×3.0	9.57	Gravel
12	1	3	1	7.05	30	38.7	65	2.3×2.3×3.0	9.57	Gravel
13	1	3	1	6.97	30	37.3	Acrylic box	2.3×2.3×3.0	9.57	Gravel
14	1	3	1	6.89	30	38	Sand mixed clay	2.3×2.3×3.0	9.57	Gravel
15A	2	2	1	6.89	30	38.5	85	2.3×2.3×3.0	9.98	Gravel
15B						37.9				A grid made of wood
16A	2	2	1	6.51	30	38.1	85	2.3×2.3×3.0	9.98	Gravel
16B						38.5				Aluminium plate
17	2	2	1	6.63	30	39.5	85	2.3×2.3×3.0	9.98	Liquefiable soil
18	1	3	1	6.95	30	38	85	2.3×2.3×3.0	11.3	Gravel
19	1	3	1	7.06	30	37.7	85	2.3×2.3×3.0	13.1	Gravel
20	1	3	1	6.93	30	38.1	85	2.3×2.3×3.0	15.5	Gravel
21	1	3	1	6.79	30	72	85	2.3×2.3×3.0	9.57	Gravel

in the native ground did not change. The relative density of the backfill for CS21 was set as high as 72% to compare the behavior of the manhole with other cases of low relative densities in backfill. The input acceleration is a sinusoidal wave with a maximum amplitude of 2.05–7.25 m/s^2 and a frequency of 1.25 Hz in prototype scale.

Table 5 classifies the test cases by the factors affecting the uplift displacement. Those factors are (a) the ground water table, (b) the amplitude of input acceleration, (c) the number of load cycles, (d) the relative density of backfill, (e) the cross-sectional area of the trench, (f) the apparent unit weight of the manhole, (g) the condition of the native ground, and (h) the contact condition between the bottom of the manhole and the trench. The above factors (a) to (h) correspond to the ones shown in the top row in Table 3. Note that, in CS13, a box made of acrylic boards (thickness = 1.1 mm) is placed to form side and bottom boundaries of the trench to simulate relatively stiff and perfectly undrained boundary conditions. The model manhole placed in the trench is put on gravels distributed at the bottom of the acrylic box. While in CS16B, the model manhole is installed directly on an aluminum plate to prevent the liquefied sand from flowing into the bottom of the manhole.

EXPERIMENTAL RESULTS AND DISCUSSIONS

Mechanism of Uplift

Based on the results obtained from the series of experiments, the mechanism of uplift is investigated in detail. Table 5 shows the summary of test results. In Table 5, residual displacement of manhole uplift measured by a laser displacement transducer indicates the maximum value in a test as shown in Figs. 9(a) and (h), while the one by hand with a ruler was measured in 1-g after rotation of the centrifuge arm was stopped. As shown in Table 5, the residual displacement measured by hand is systematically smaller than the ones measured by a laser dis-

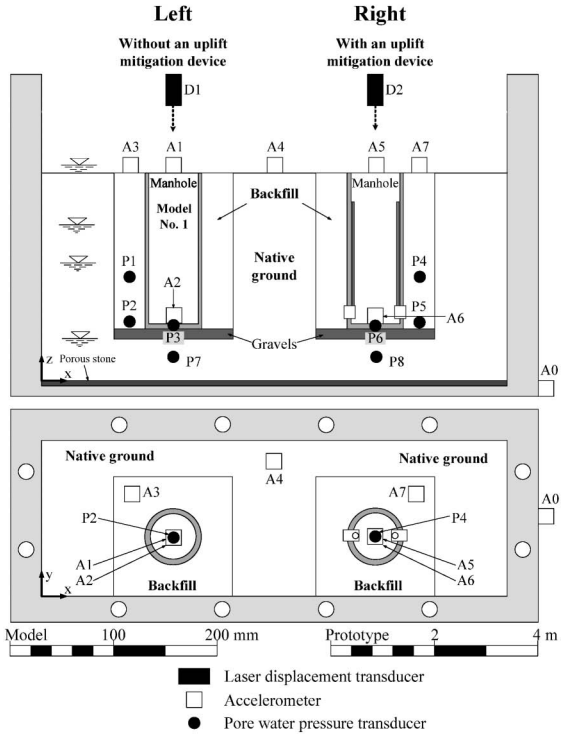

Fig. 7. Representative centrifuge model set-up for CS1 to CS12

Fig. 8. Uplifted manhole after shaking (CS3)

placement transducer. This might be because the model manhole sunk down as excess pore water pressure dissipated in the trench backfill by the time when the centrifuge arm had made a full stop.

Figure 9 shows time histories recorded for CS3 (Figs. 9(a)–(g)), whose ground water table is located at GL −1.0 m, and for CS4 (Figs. 9 (h)–(n)), whose ground water table is located at GL −1.7 m. Maximum peak accelerations measured in each case are 7.15 m/s^2 and 7.19 m/s^2, respectively. The magnitude of the uplift displacement of CS4, 0.488 m, is almost half that of CS3, 0.952 m, which has a shallower ground water table (Figs. 9(a) and (h)). As shown in Fig. 9(a), the manhole started to lift up at 5.8 s when the excess pore water pressure measured in the middle (P1) (Fig. 9(b)) and at the bottom (P2) (Fig. 9(c)) of the backfill were still under the initial effective vertical stress indicated by σ'_v. At 5.8 s, excess pore water pressure at the bottom of the manhole (Fig. 9(d): P3) has already exceeded the initial effective vertical stress (σ'_{vm}), 9.11 kPa, which is significantly smaller than that of P2, 31.4 kPa. This indicates that the bottom of the backfill initially liquefies, and as shaking continues, the liquefied area expands to the entire backfill under water. The initial pressure difference, P2 − P3 = 31.4 − 9.11 = 22.3 kPa, may be the primary cause of the manhole uplift.

Table 4. Summary of manhole uplift and backfill settlements

Test No.	Type of model manhole	Manhole uplift		Backfill settlement
		Laser disp. transducer	Hand measurement	
	No.	m	m	m
1	1	Out of range	1.100	0.183
2	1	0.958	0.850	0.190
3	1	0.952	0.860	0.200
4	1	0.488	0.450	0.180
5	1	0.000	0.000	0.050
6	1	0.000	0.000	0.073
7	1	0.201	0.170	0.175
8	1	1.074	0.810	0.217
9	1	0.000	0.020	0.018
10	1	0.234	0.200	0.168
11	1	Out of range	1.600	0.220
12	1	Out of range	1.030	0.170
13	1	0.231	0.220	0.230
14	1	0.822	0.740	0.205
15A	2	0.503	0.460	0.200
15B		0.479	0.479	0.188
16A	2	0.518	0.470	0.150
16B		0.285	0.285	0.133
17	2	0.602	0.510	0.148
18	1	0.574	0.540	0.178
19	1	0.421	0.370	0.168
20	1	0.131	0.110	0.150
21	1	0.129	0.120	0.023

Table 5. Factors considered in the experiments, corresponding test cases and figure numbers

	Factors	Test No.	Figures
(a)	Ground water level (GWL)	1, 2, 3, 4, 5, 15A, 16A	Fig. 12(a)
(b)	Max. amplitude of input acc.	2, 3, 6, 7	Fig. 12(b)
(c)	Number of load cycles	2, 3, 10, 11	Fig. 12(c)
(d)	Relative density of backfill	2, 3, 9, 21	Fig. 12(d)
(e)	Cross-sectional area of trench	2, 3, 8	Fig. 12(e)
(f)	Apparent unit weight of manhole	2, 3, 18, 19, 20	Fig. 12(f)
(g)	Condition of native ground	2, 3, 8, 12, 13, 14	Fig. 15
(h)	Contact condition at the bottom of a manhole	15AB, 16AB, 17	Fig. 17

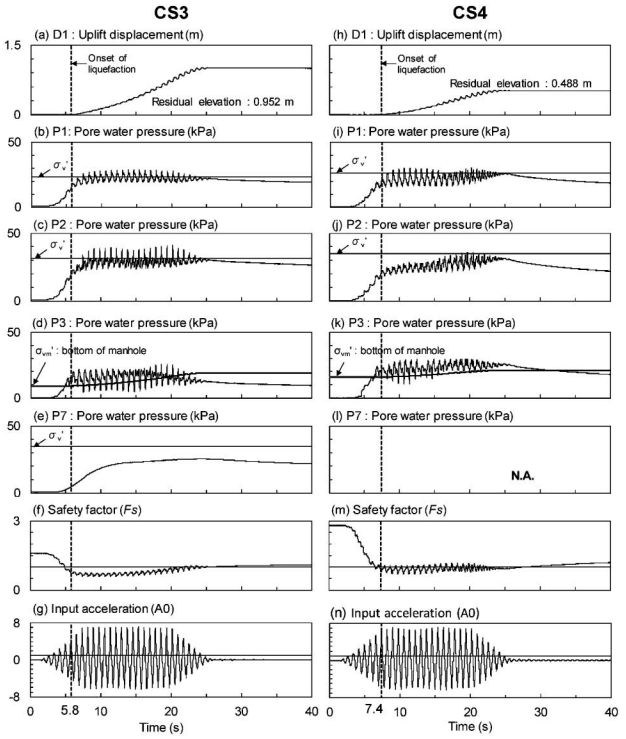

Fig. 9. Time histories of (a) uplift displacement, (b)–(e) excess pore water pressure (P1 to P3, and P7), and (f) safety factor for CS3, and (g) to (l) for CS4

Namely, once liquefied, the backfill soil near the bottom of the manhole has the potential to move toward just under the manhole. As shown in Figs. 9(h) to (k), the same trend can be seen for CS4. In both Figs. 9(d) and (k), when the manhole is uplifting, the excess pore water pressure measured at the bottom of the manhole, P3, exceeds the effective vertical stress computed by taking into account the manhole uplift (Eq. (1)). This indicates that the liquefied backfill under the manhole is anisotropic stress condition which causes the uplifting force until the equilibrium of the vertical forces is achieved. Thus, the large excess pore water pressure acting on the bottom surface of the manhole may be one of the causes of the manhole uplift. In Figs. 9(d) and (k), the effective vertical stress at the bottom of the manhole, σ'_{vm}, is computed by the following equation:

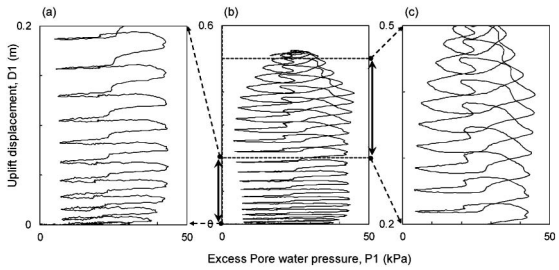

Fig. 10. Relationship between uplift displacement (D1) and excess pore water pressure (P1) for CS4: (a) beginning of uplift: 0 m–0.2 m, (b) entire record: 0 m–0.6 m, (c) towards end of uplift: 0.2 m–0.5 m

$$\sigma'_{vm} = \gamma_m(h_w + \Delta f) + \gamma'_m(h - h_w - \Delta f), \quad (1)$$

where

γ_m: the apparent unit weight of the manhole (Table 1), which is a function of the shape of the manhole;

$\gamma'_m = \gamma_m - \gamma_w$: the submerged unit weight of the manhole;

γ_w: the unit weight of water;

h: manhole length;

h_w: ground water depth in backfill; and

Δf: uplift displacement of a manhole measured during experiments.

However, if the liquefied area in the backfill is limited, say, to only the area near the bottom of the manhole, the frictional force acting on the side may be large enough to keep the manhole undisturbed.

The manhole uplift stopped and the manhole itself started to sink down just after shaking, except for CS13, CS14 and CS21. As shown in Table 3, in CS13, the backfill was confined in the acrylic board, in CS14, the native ground was made of sand mixed with clay, and in CS21, the backfill was compacted at 72% of the relative density. In CS21, the manhole uplift was 0.117 m just after the shaking, then it increased to 0.129 m at about 67 s after shaking. The differences in the permeability and stiffness at the boundary may contribute to the continuous uplift after shaking.

Next, to see the effect of shaking on the uplift, uplift displacement (D1) is plotted against excess pore water pressures, P1, for CS4 (Fig. 10). Figure 10(b) shows the entire process, and Figs. 10(a) and (c) depict the enlarged section at the beginning and ending of shaking, respectively. As seen in Fig. 10(a), in the beginning of the uplift, the curve shows that the manhole continues to uplift regardless of fluctuation of the excess pore water pressure. As shaking continues (Fig. 10(c)), the curves start to draw loops induced probably by the rocking of the manhole with the shaking, which is associated with the low confining stress acting on the manhole.

To see the residual deformation of the ground after shaking, the model ground of CS1 is vertically cut at the center of the trench (Fig. 11). In the model ground, colored sands are sandwiched to see the ground deformation (Fig. 11(a)). As shown in Fig. 11(b), the model manholes are tilted due to large amount of uplift, and the backfill soil at the bottom of the manhole moves toward

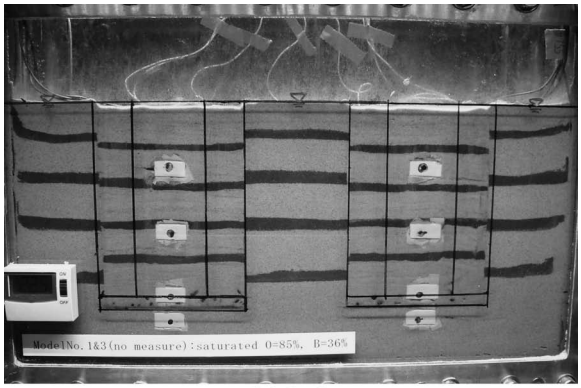

(a) before

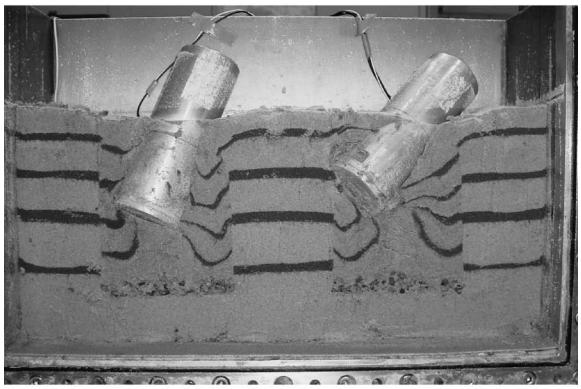

(b) after

Fig. 11. Deformation of the model ground before (a) and after (b) shaking for CS1. In (b), the model ground is cut on the vertical plane

the bottom of the uplifted manhole. This clearly shows that the uplift is caused by the flow of liquefied backfill to underneath the manhole. On the other hand, native ground is only slightly deformed toward the trench near the ground surface.

Safety Factor and Uplift Displacement

Forces acting on a manhole are the weight of the manhole and the frictional force at the side of the manhole, both pointing downward, and the hydrostatic force and the force due to the excess pore water pressure, which point upward. In what follows, the safety factor, F_s, written below, is evaluated by considering the equilibrium of forces acting on a manhole:

$$F_s = \frac{M+R}{U+H} = \frac{d\gamma_m(h,\ d)h + \pi K(d/2)h_w^2\gamma_t \tan\delta}{dr_u\{\gamma_t h_w + \gamma'(h-h_w-\Delta f)\} + d\gamma_w(h-h_w-\Delta f)}, \quad (2)$$

where

M: the weight of manhole;

R: frictional force between backfill and sidewall of a manhole, assumed only in the non-liquefied layer above the ground water table, and derived as follows; where a manhole is assumed to be a cylinder, and z is the coordinate pointing downward along with the manhole length and having $z=0$ at the ground surface, and θ is the center angle of a cylinder in horizontal section.

$$R = N\tan\delta = \left[\int_0^{2\pi}\int_0^{h_w}\{(K\gamma_t z)dz\}\frac{d}{2}d\theta\right]\tan\delta = K\gamma_t\frac{h_w^2}{2}\frac{d}{2}\int_0^{2\pi}d\theta\tan\delta = \pi K(d/2)h_w^2\gamma_t\tan\delta \quad (3)$$

U: uplifting force due to liquefaction;

H: the buoyant force due to hydrostatic pressure;

K: a coefficient of lateral earth pressure ($=0.5$);

δ: the friction angle between manhole and backfill ($=10°$);

r_u: excess pore water pressure ratio;

γ_t: the unit weight of backfill above the groundwater table; and

$\gamma' = \gamma_{sat} - \gamma_w$: the submerged unit weight of backfill.

In computation, the value of P1 is used. As shown in Figs. 9(f) and (m), the safety factors of CS3 and CS4 before shaking are, respectively, 1.6 and 2.8, and they decrease with the increase of the excess pore water pressure in the backfill (P1). The manhole starts to lift up when the safety factor becomes 0.72 for CS3. For CS4, it is 0.81. Then, with the manhole uplift, the safety factors slightly increase. When the uplifting stops, the safety factor becomes close to 1, as is expected. Final uplift displacements of CS3 and CS4 are, respectively, 0.952 m and 0.488 m, and the corresponding initial safety factors are 1.6 and 2.8. Although the manhole with the small initial safety factor had more uplift in this particular test, this may not always be the case because of uncertainty related to properties of input motion.

Factors Affecting the Uplift Displacement

In Fig. 12, test results are plotted in terms of the normalized uplift of a manhole ($\Delta f/h$: uplift ratio) and backfill settlement ($\Delta s/h$: settlement ratio) vs. factors listed in Table 5. In Fig. 12(a), for example, when the ground water table coincides with the ground surface, the uplift ratio is 0.37, and this decreases with the increase of the normalized depth of the ground water table (h_w/h). The settlement ratio shows a similar trend with the uplift ratio. The amplitude and number of load cycles of input acceleration also show strong correlation with the uplift and settlement (Fig. 12(b) and (c)). From Fig. 12(c), the uplift displacement of CS11 may have reached its maximum value, $\Delta f/h = 0.53$ which is the largest value among the experiments carried out in this study. Properties of backfill—relative density of backfill and trench width—are investigated, respectively, in Figs. 12(d) and (e). As shown in Fig. 12(d), compaction of backfill material greatly reduces the amount of uplift and settlement, while the trench width has less effect. The unit weight of a manhole is examined in Fig. 12(f). As the unit weight of the manhole approaches the saturated unit weight of backfill material ($\gamma_m = \gamma_{sat}$), the uplift displacement reduces, while settlement is not much affected. Based on the results ob-

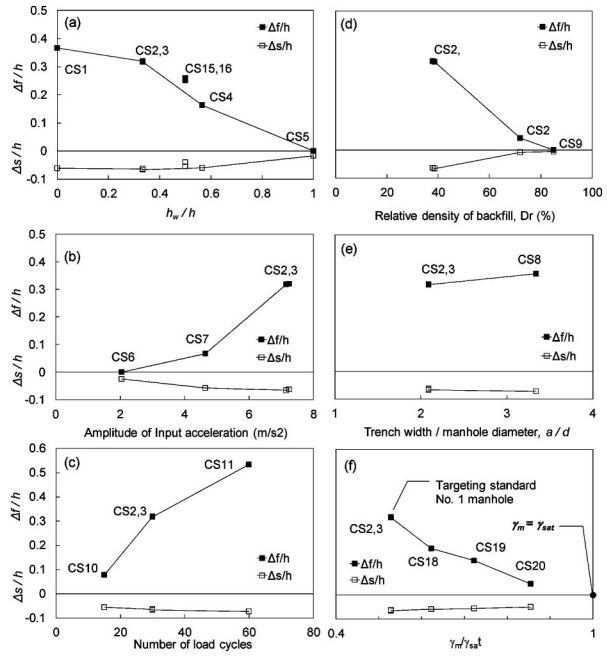

Fig. 12. Relationship among uplift ratio ($\Delta f/h$), settlement ratio ($\Delta s/h$) and factors affecting manhole uplift: (a) ground water table, (b) amplitude of input acceleration, (c) number of load cycles, (d) relative density of backfill, (e) cross-sectional area of a trench, and (f) apparent unit weight of a manhole

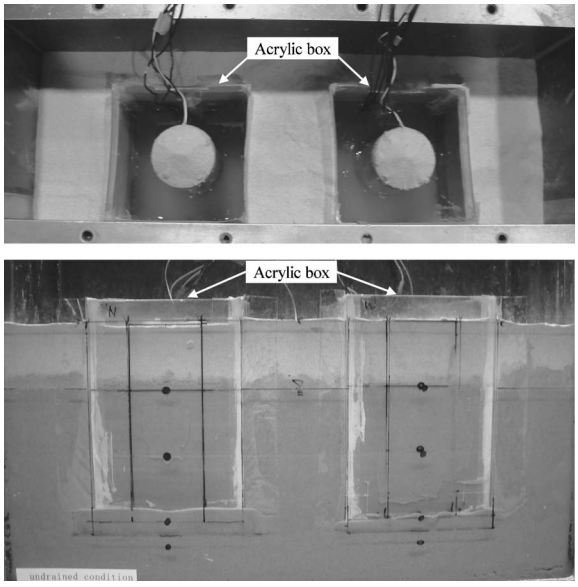

Fig. 13. A view of the model manhole and trench with acrylic box (CS13)

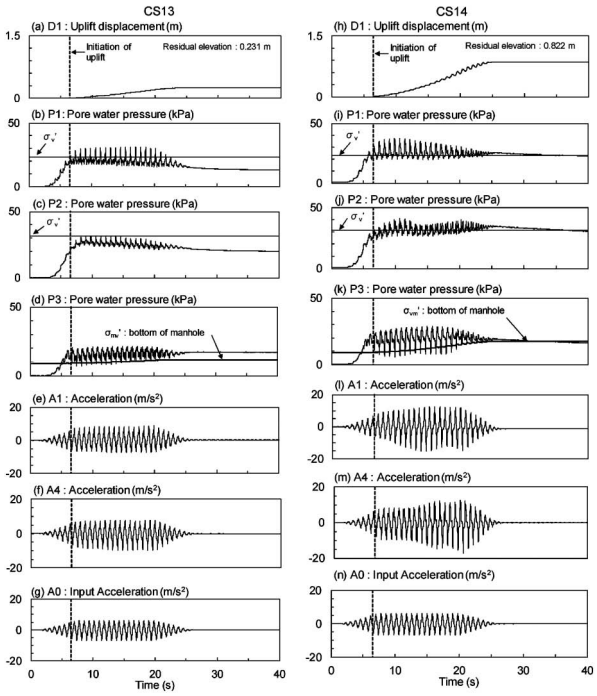

Fig. 14. Time histories of (a) uplift displacement, (b)–(d) excess pore water pressure (P1 to P3), and (e)–(g) acceleration (A1, A4, and A0) for CS13, and (h) to (n) for CS14

tained above, the compaction of a trench backfill may be the best option to mitigate against uplift (Fig. 12(d)).

Condition of the Native Ground and Manhole Uplift

To evaluate the effects of native ground, test cases of CS2, CS3, CS8, CS12, CS13, and CS14 are compared. For all of the selected test cases, the relative density of the backfill is kept nearly constant (36%) (Table 3). For CS2 and CS3, the relative density of the native ground is 85%, while for CS12 and CS8 it is adjusted to 65% and 36%, respectively. In CS13, the acrylic box mentioned earlier (Fig. 13) is employed. The material of the native ground in CS14 is a mixture of sand (85%) and the DL Clay (25%) with a permeability of 9.81×10^{-5} cm/s, which is 1/37 of the sand with 85% relative density.

As shown in Fig. 9(e): with regard to excess pore water pressure in the native ground (P7), although it was well compacted to about 85% of the relative density, there was a significant increase in the excess pore water pressure buildup (max. effective pore water pressure ratio = 0.72). If this increase was to occur at shallower depth near the ground surface where no pore pressure transducer was installed in the study, the ground might have suffered large deformation which might induce deformation of the trench.

Figure 14 shows time histories obtained after CS13 and CS14. When the backfill is confined by the acrylic boards (CS13), the backfill is nearly liquefied (Fig. 14(b) and (c)), while the acceleration amplitude on the top of the manhole and surface of the native ground show no significant reduction or amplification due to liquefaction. A possible explanation of the uplift with the acrylic board might be that the deformation, such as squeezing, of the trench backfill was minimized. When the native ground is made of well compacted sand mixed with clay material, manhole uplift is large (0.822 m) and the acceleration on the top of the manhole and native ground surface show significant amplification, which is probably due to the deformation of the ground surface associated with liquefaction of the trench backfill. Due to the lack of pore water pres-

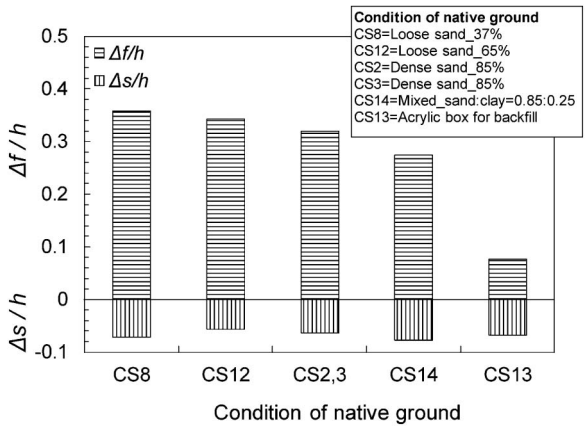

Fig. 15. Relationship among uplift ratio ($\Delta f/h$), settlement ratio ($\Delta s/h$) and condition of native ground

sure measurements near the ground surface of native ground, it is difficult to judge whether the native ground made of sand mixed with clay was liquefied.

In 1-G shaking table tests, Koseki, et al. (1997) compared a manhole's final uplift displacement for the cases ''with'' and ''without'' a vinyl sheet that formed an impermeable vertical and flexible interface between the backfill and native ground. They found large uplift in the case with a vinyl sheet, and suggested that the sheet increased the degree of liquefaction in the backfill. The results of the present study suggest that not only the excess pore water pressure exerted in the backfill but also shear deformation or slight squeezing of the backfill might contribute to the large magnitude of the uplift.

Figure 15 compares the uplift ratio under conditions of the native ground described above. The maximum uplift ratio (0.36) is observed when the native ground is loose (CS8: $Dr = 36\%$). Then, the uplift ratio is slightly reduced with the increase of the relative density (CS12: $Dr = 65\%$ CS2, and CS3: $Dr = 85\%$), and the minimum uplift ratio (0.08) is observed with the acrylic box, although the excess pore water pressure was fully built up in the box. This might be because the shear deformation of the trench backfill induced by the deformation of the native ground was minimized by the existence of the box.

Contact Condition at the Bottom of the Manhole

The uplift displacement may also be influenced by the contact conditions beneath the manhole. The conditions considered are as follows: (1) partial contact condition by a grid made of wooden lattice (Fig. 16(a)); (2) perfect contact condition by placing the manhole on a flat aluminum plate put at the bottom of the trench, which prevents liquefied sands from flowing from the bottom of the manhole (Fig. 16(b)); (3) gravels; and (4) loose liquefiable soil. In field construction, manholes are normally placed on a grid made of wooden lattice or gravels. As shown in Fig. 17, the minimum uplift ratio, 0.14, is obtained with the use of an aluminum plate (CS16B), and the maximum uplift ratio, 0.30, is obtained for the case of liquefiable soil (CS17). The uplift ratios of the manholes on gravels

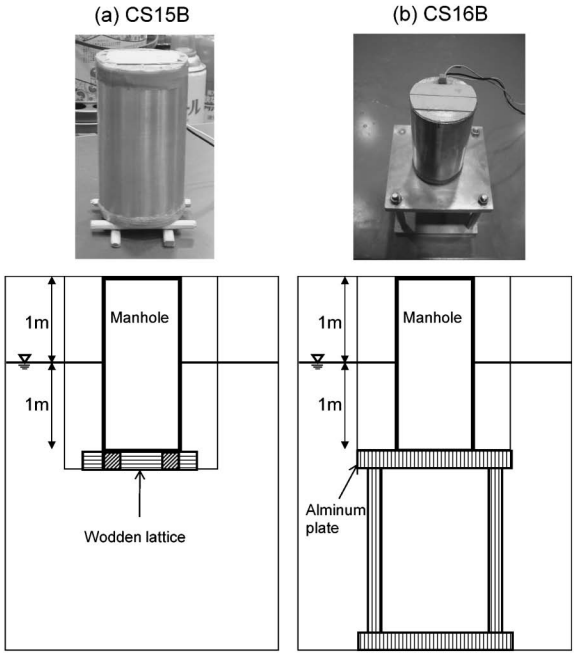

Fig. 16. Devices placed under the model manhole: (a) a grid of wooden lattice and (b) aluminum plate for prevention of liquefied sands from flowing from surrounding backfill

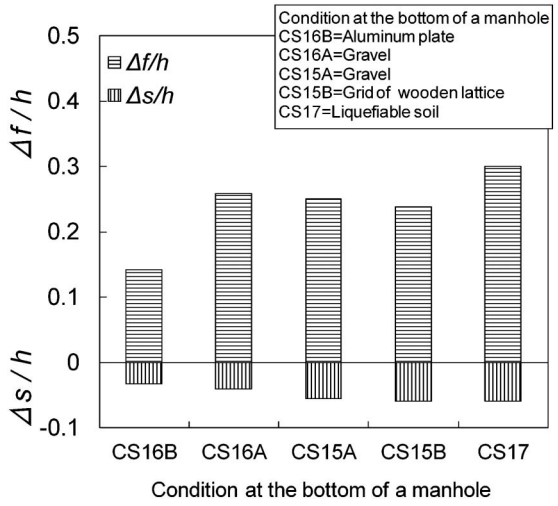

Fig. 17. Relationship among uplift ratio ($\Delta f/h$), settlement ratio ($\Delta s/h$) and ground condition under the manhole

and the grid are nearly at the same level. With a metal plate, which prevents liquefied soils from moving toward the bottom of the manhole, the uplift ratio is reduced to about half of what it is for the other cases. The results show that liquefaction just under the manhole may have a large influence on the uplift behavior of a manhole.

SUMMARY AND CONCLUSIONS

Centrifuge studies were performed to study the mechanism of manhole uplift and to investigate the various factors affecting the manhole uplift in liquefied backfill. In the tests, it was clearly observed that liquefied

backfill flows into the bottom of the manhole during uplifting. Combining this observation with measurements carried out in the study, with regard to the uplift mechanism of a manhole, it can be concluded that the existence of the overburden pressure difference between the bottom of the manhole and, at the same depth, of the backfill may be the primary cause of the manhole uplift. In addition to this, the intensity of the input motion and the deformation of the trench backfill may have a significant influence on manhole uplift.

The safety factor was evaluated in relation to the uplift displacement. Although a manhole with a small initial safety factor had more uplift in the presented cases, this is not always the case because of uncertainty related to properties of input motion.

The test results were investigated in terms of the normalized uplift and settlement vs. factors that might have influence on the uplifts and settlements. The factors considered in the tests are as follows: (a) the depth of the ground water table, (b) the amplitude of input acceleration, (c) the number of load cycles, (d) the relative density of backfill, (e) the cross-sectional area of a trench, (f) the apparent unit weight of the manhole, (g) the condition of the native ground, and (h) the contact conditions between the bottom of the manhole and the trench. All of these factors showed strong correlation with the manhole uplift and backfill settlements, except for ''(e) the cross-sectional area of a trench, a/d'' which showed only minor variation. From a practical point of view, compaction of the trench backfill may be the best option to mitigate against uplift.

Investigation of the native ground condition revealed that the largest manhole uplift was observed when the native ground is loose. Although the excess pore water pressure was fully built up, minimum uplift was observed in the case where the acrylic box was used as a boundary between backfill and native ground to have a stiff and perfectly undrained boundary condition. This may suggest that not only the excess pore water pressure exerted in the backfill but also the shear deformation of the backfill may have a significant influence on manhole uplift. Various contact conditions between the bottom of a manhole and trench base were investigated to see the effects on the uplift. It was found that a perfect contact condition created by placing the manhole on a flat aluminum plate gave minimum uplift, and the condition with liquefiable soil at the bottom of a manhole gave maximum uplift. Thus, liquefaction just under the manhole may be an important factor to be considered in the uplift behavior of a manhole.

REFERENCES

1) Dewoolkar, M. M., Ko, H.-Y., Stadler, A. T. and Astaneh, S. M. F. (1999): A substitute pore fluid for seismic centrifuge modeling, *Geotechnical Testing Journal*, ASTM, **22**(3), 196–210.
2) Iai, S. and Matsunaga, Y. (1991): Mechanism of uplift of structures due to liquefaction, *International Symposium on Natural Disaster Reduction and Civil Engineering*, JSCE, 297–306.
3) JGS (2003): Uplift behavior and damage of underground structures caused by liquefaction, *Report to The 48th Geotechnical Engineering Symposium*, 115.
4) JGS (2004): Reconnaissance report on the 2003 Tokachi-oki earthquake, *Japanese Geotechnical Society* (in Japanese).
5) JSSMFE (1994): Research report of damage caused by the 1993 Kushiro-oki Earthquake and the Noto-hanto-oki Earthquake, *Japanese Society of Soil Mechanics and Foundation Engineering*, 289–303 (in Japanese).
6) JSWA (2001): Guideline and manual for planning and design in sewerage systems, *Japan Sewege Works Association* (in Japanese).
7) Kang, G. C. (2010): Assessing uplift displacement of buried geotechnical structures in liquefied ground during earthquakes, *PhD thesis*, Department of Civil and Earth Resources Engineering, Kyoto University, Japan.
8) Kiku, H., Yasuda, S., Tanaka, T. and Itou, T. (2004): Damage of sewerage systems in Toyokoro town during the 2003 Tokachi-oki, Japan, Earthquake, *The 59th Japan National Conference on Civil Engineering*, 423–424 (in Japanese).
9) Koseki, J., Matsuo, O. and Koga, Y. (1997): Uplift behavior of underground structures caused by liquefaction of surrounding soil during earthquake, *Soils and Foundations*, **37**(1), 97–108.
10) Koseki, J., Matsuo, O., Ninomiya, Y. and Yoshida, T. (1997): Uplift of sewer manhole during the 1993 Kushiro-Oki earthquake, *Soils and Foundations*, **37**(1), 109–121.
11) Koseki, J., Matsuo, O. and Tanaka, S. (1998): Uplift of sewer pipes caused by earthquake-induced liquefaction of surrounding soil, *Soils and Foundations*, **38**(3), 75–87.
12) Ohtomo, K., Tohma, J. and Iwatate, T. (1987): Investigation on mitigation of liquefaction disaster for underground structures (part 2)—evaluation of uplift stability of buried pipe and application of gravel drain to prevent liquefaction—, *Central Research Institute of Electric Power Industry, Report No. U86027* (in Japanese).
13) Okamoto, S. (1984): *Introduction to Earthquake Engineering*, second edition, University of Tokyo Press, 88.
14) RION Co. (1997): Viscotester Brochure, VT-03F, Higashimotomachi, Kokubunji, Tokyo, Japan.
15) Shin-Etsu Chemical Co. (1997): Metolose Brochure, Cellulose Dept., 6–1, Ohtemachi 2-chome, Chiyoda-ku, Tokyo, Japan.
16) Tobita, T., Ghayamghamian, M. R., Iai, S. and Kang, G.-C. (2007): Preliminary report of the Niigataken Chuetsu-oki, Japan, Earthquake in 2007, *Journal of Japan Society of Natural Disaster Science*, **26**(2), 215–223 (in Japanese).
17) Tobita, T., Kang, G. C. and Iai, S. (2010): Uplift behaviour of buried structures under strong shaking, *7th International Conference on Physical Modelling in Geotechnics (ICPMG 2010)*, Springman, (eds. by Laue and Seward), 1439–1444.
18) Wakamatsu, K. (2007): Liquefaction-induced damage during near-field earthquakes in the Tokyo metropolitan area, *Journal of Geography*, **116**(3/4), 480–489 (in Japanese).
19) Yasuda, S., Nagase, H., Itafuji, S., Sawada, H. and Mine, K. (1995): A study on the mechanism of the floatation of buried pipes due to liquefaction, *Soil Dynamics and Earthquake Engineering VII*, Transaction on the built environment 14, 125–132.
20) Yasuda, S., Morimoto, I., Kiku, H. and Tanaka, T. (2004): Reconnaissance report on the damage caused by three Japanese earthquakes in 2003, *Proc. of the 3rd International Conference on Earthquake Geotechnical Engineering and 11th International Conference on Soil Dynamics & Earthquake Engineering*, Key note lecture, 1, 14–21.
21) Yasuda, S. (2005): Allowable displacement of the ground at the aspect of traffic flow after the 2004 Niigata-ken Chuetsu-ken, Japan, Earthquake, *The Japan National Conference on Earthquake Engineering*, 146–147.
22) Yasuda, S. and Kiku, H. (2006): Uplift of sewage manholes and pipes during the 2004 Niigataken-Chuetsu earthquake, *Soils and Foundations*, **46**(6), 885–894.
23) Yasuda, S., Tanaka, T. and Kiku, H. (2009): Uplift of sewage manhole during 1993 Kushiro-oki EQ., 2003 Tokachi-oki EQ. and 2004 Niigataken Chuetsu EQ, *Earthquake Geotechnical Case Histories for Performance-based Design*, Taylor & Francis Group, London,

95–108.
24) Yasuda, S., Verdugo, R., Konagai, K., Sugano, T., Villalobos, F., Okamura, M., Tobita, T., Torres, A. and Towhata, I. (2010): Geotechnical damage caused by the 2010 Maule, Chile earthquake, *ISSMGE Bulletin*, **4**(2), 16–27.